PHYSICAL REVIEW D **78,** 096010 (2008)

# Saturation in deep inelastic scattering from the AdS/CFT correspondence

Lorenzo Cornalba[1,2] and Miguel S. Costa[3]

[1]*Centro Studi e Ricerche E. Fermi Compendio Viminale, I-00184, Roma, Italy*

[2]*Università di Milano-Bicocca and INFN, Sezione di Milano-Bicocca Piazza della Scienza 3, I-20126 Milano, Italy*

[3]*Departamento de Física e Centro de Física do Porto, Faculdade de Ciências da Universidade do Porto, Rua do Campo Alegre 687, 4169-007 Porto, Portugal*

(Received 9 June 2008; published 17 November 2008)

We analyze deep inelastic scattering at small Bjorken $x$, using the approximate conformal invariance of QCD at high energies. Hard Pomeron exchanges are resummed eikonally, restoring unitarity at large values of the phase shift in the dual anti-de Sitter (AdS) geometry. At weak coupling this phase is imaginary, corresponding to a black disk in AdS space. In this saturated regime, cross sections exhibit geometric scaling and have a simple universal form, which we test against available experimental data for the proton structure function $F_2(x, Q^2)$. We predict, in particular, the dependence of the cross section on the scaling variable $(Q/Q_s)^2$ in the deeply saturated region, where $Q_s$ is the usual saturation scale. We find agreement with current data on $F_2$ in the kinematical region $0.5 < Q^2 < 10$ GeV$^2$, $x < 10^{-2}$, with an average 6% accuracy. We conclude by discussing the relation of our approach with the commonly used dipole formalism.

DOI: 10.1103/PhysRevD.78.096010 PACS numbers: 13.60.Hb, 11.25.Hf, 11.25.Tq

## I. INTRODUCTION

The high energy behavior of QCD is greatly simplified by the asymptotic weakness of the coupling and the approximate conformal invariance of the theory. Of great interest, in this respect, is the study of interaction processes in the Regge limit of high center of mass energy, with the other kinematical invariants kept fixed. This kinematical regime is, for instance, relevant to the analysis of deep inelastic scattering (DIS) experiments at fixed photon virtuality $Q^2$ in the limit of vanishing Bjorken $x$.

To the extent that QCD can be approximated by a conformal field theory (CFT), we must, in general, analyze CFT correlators of the form

$$\langle \mathcal{O}_1(q_1)\mathcal{O}_2(q_2)\mathcal{O}_1^\star(q_3)\mathcal{O}_2^\star(q_4)\rangle \tag{1}$$

in the limit of large $s = -(q_1 + q_2)^2$ and at fixed virtualities $Q_i^2 = q_i^2$ and momentum transfer $t = -(q_1 + q_3)^2$. In the high energy limit, the correlator (1) is best analyzed in impact parameter space. The correct representation is suggested by the AdS/CFT duality [1], although let us stress that all of the results in this paper are purely based on simple implications of conformal symmetry and could be derived also in the field theory language. Considering (1) as a high energy process in $AdS_5$, the relevant transverse space is then the three-dimensional hyperbolic space $H_3$, holographically dual to the usual two-dimensional plane transverse to the high energy process described by (1), as shown in Fig. 1. Representing four-dimensional vectors as $(x^+, x^-, \mathbf{x})$, with $x^\pm$ light cone variables and $\mathbf{x}$ a two-dimensional transverse vector, we can parametrize $H_3$ using Poincaré coordinates $\rho, \mathbf{x}$ with metric $\rho^{-2}(d\rho^2 + d\mathbf{x}^2)$ and volume form $\rho^{-3}d\rho d^2\mathbf{x}$, with $\rho > 0$ the distance to the holographic boundary of $H_3$. Following the results in [2–10], we may write the impact parameter representation for the correlator (1). Choosing, for simplicity of exposition, external scalar operators, it is given by

$$2s\int d^2\mathbf{b}e^{i\mathbf{b}\cdot\mathbf{q}}e^{2i\delta(s,\mathbf{b})}, \tag{2}$$

where $\mathbf{q}$ is the transverse momentum transfer with $-t = \mathbf{q}^2$ and where $\mathbf{b}$ is the usual impact parameter. The phase

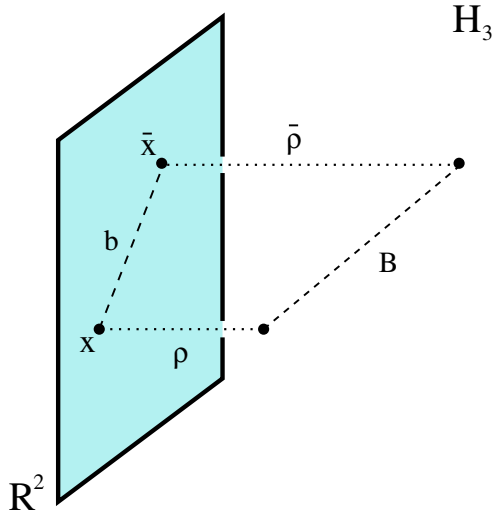


FIG. 1 (color online). Impact points $\rho, \mathbf{x}$ and $\bar\rho, \bar{\mathbf{x}}$ in $H_3$, separated by a geodesic distance $B$. Dropping the radial coordinates $\rho$ and $\bar\rho$, we obtain the impact points $\mathbf{x}$ and $\bar{\mathbf{x}}$ in the plane transverse to the high energy process $R^2$, with impact parameter $\mathbf{b} = \mathbf{x} - \bar{\mathbf{x}}$.

*Lorenzo.Cornalba@mib.infn.it
+miguelc@fc.up.pt

 

shift $\delta(s, \mathbf{b})$ is itself given by

$$e^{2i\delta(s,\mathbf{b})} = \int \frac{d\rho}{\rho^3} f_1(\rho) f_3(\rho) \int \frac{d\bar{\rho}}{\bar{\rho}^3} f_2(\bar{\rho}) f_4(\bar{\rho}) e^{2i\Delta(S,B)}, \tag{3}$$

with $\Delta(S, B)$ the phase shift in anti-de Sitter (AdS) space, which depends on the AdS energy squared and impact parameter $S$ and $B$, according to[1]

$$S = \rho\bar{\rho}s, \qquad \cosh B = \frac{\rho^2 + \bar{\rho}^2 + \mathbf{b}^2}{2\rho\bar{\rho}}. \tag{4}$$

In particular, $B$ is the geodesic distance between the points $\rho, \mathbf{x}$ and $\bar{\rho}, \bar{\mathbf{x}}$ in $H_3$, with $\mathbf{b} = \mathbf{x} - \bar{\mathbf{x}}$. These represent the impact points of the operators $\mathcal{O}_1$ and $\mathcal{O}_2$ in the transverse space. Finally, the functions $f_i$ are the radial wave functions for the scattering states. For scalar operators $\mathcal{O}_1$ and $\mathcal{O}_2$ of dimension $\Delta_1$ and $\Delta_2$, they are given by $f_i \propto Q_i \rho^2 K_{\Delta_1 - 2}(Q_i \rho)$ for $i = 1, 3$ and by $f_i \propto Q_i \bar{\rho}^2 K_{\Delta_2 - 2}(Q_i \bar{\rho})$ for $i = 2, 4$ [11]. We normalize the wave functions so that

$$\int \frac{d\rho}{\rho^3} f_1(\rho) f_3(\rho) = \int \frac{d\bar{\rho}}{\bar{\rho}^3} f_2(\bar{\rho}) f_4(\bar{\rho}) = 1. \tag{5}$$

As shown in [5], the impact parameter representation (2) and (3) approximates the conformal partial wave decomposition of the correlator (1) in the channel $\mathcal{O}_1\mathcal{O}_2 \to \mathcal{O}_1^\star\mathcal{O}_2^\star$, with intermediate states of conformal dimension and spin, respectively, given by $\sqrt{S}\cosh(B/2)$ and $\sqrt{S}\sinh(B/2)$. In analogy with the usual results for scattering in flat space, we then expect that AdS unitarity implies [9,10]

$$\mathrm{Im}\,\Delta(S, B) \geq 0,$$

even though the phase shift $\delta(s, \mathbf{b})$ does not satisfy a simple unitarity constraint.

We shall focus, for concreteness, on the very relevant and simple case of vanishing momentum transfer $\mathbf{q} = 0$ and equal virtualities for the incoming and outgoing states $Q = Q_1 = Q_3$ and $\bar{Q} = Q_2 = Q_4$. It is then natural to construct, from the correlator (2), the following effective cross section:

$$\Sigma(s, Q, \bar{Q}) = 2 \int d^2\mathbf{b}\, \mathrm{Re}(1 - e^{2i\delta(s,\mathbf{b})}).$$

Using (3), the cross section $\Sigma$ can be conveniently written as

$$2 \int \frac{d\rho}{\rho^3} f_1(\rho) f_3(\rho) \int \frac{d\bar{\rho}}{\bar{\rho}^3} f_2(\bar{\rho}) f_4(\bar{\rho}) \sigma(s, \rho, \bar{\rho}), \tag{6}$$

where we have defined the unintegrated cross sections

$$\sigma(s, \rho, \bar{\rho}) = \int d^2\mathbf{b}\, \sigma(s, \rho, \bar{\rho}, \mathbf{b}),$$
$$\sigma(s, \rho, \bar{\rho}, \mathbf{b}) = \mathrm{Re}(1 - e^{2i\Delta(S,B)}). \tag{7}$$

In this language, $\sigma(s, \rho, \bar{\rho}, \mathbf{b})$ is the natural object which automatically satisfies the unitarity bound $0 \leq \sigma \leq 2$ due to AdS unitarity $\mathrm{Im}\Delta \geq 0$. Moreover, for a black disk region we have $\sigma \to 1$, corresponding to a phase shift $\Delta$ with a large imaginary part.

In general, we cannot evaluate the integral over the impact parameter $\mathbf{b}$. We may, on the other hand, use the relation (4) between $\mathbf{b}$ and the AdS impact parameter $B$ to rewrite the cross section $\sigma(s, \rho, \bar{\rho})$ in (7) as

$$\sigma(s, \rho, \bar{\rho}) = 2\pi\rho\bar{\rho} \int_{|\ln(\bar{\rho}/\rho)|}^{\infty} dB \sinh B\, \mathrm{Re}(1 - e^{2i\Delta(s\rho\bar{\rho},B)}). \tag{8}$$

It is now apparent that we are probing the phase $\Delta(S, B)$ for fixed $S = s\rho\bar{\rho}$ and for $B \geq |\ln(\bar{\rho}/\rho)|$. Finally, note that the unintegrated cross sections satisfy, due to conformal invariance, nontrivial relations under the transformation $\rho \to \bar{\rho}^2/\rho$ with $s \to s(\rho^2/\bar{\rho}^2)$, $\mathbf{b} \to \mathbf{b}(\bar{\rho}/\rho)$, which leave invariant $S$ and $B$. More precisely, $\sigma(s, \rho, \bar{\rho}, \mathbf{b})$ is invariant, whereas

$$\frac{\rho^2}{\bar{\rho}^2} \sigma\left(s \frac{\rho^2}{\bar{\rho}^2}, \frac{\bar{\rho}^2}{\rho}, \bar{\rho}\right) = \sigma(s, \rho, \bar{\rho}).$$

The phase shift $\Delta(S, B)$ depends both on the number of colors $N$ and on the 't Hooft coupling $\bar{\alpha}_s = \alpha_s N/\pi$ of the theory. For large energy squared and impact parameter $S$ and $B$, the phase $\Delta$ will be dominated by the leading Regge pole of the planar diagrams of the theory [9,10] and will have a general representation of the form[2]

$$\Delta(S, B) = \frac{1}{N^2} \int d\nu \beta(\nu) S^{j(\nu)-1} \Omega_{i\nu}(B), \tag{9}$$

where the Regge spin $j(\nu)$ and residue $\beta(\nu)$ depend implicitly only on the 't Hooft coupling $\bar{\alpha}_s$ and are even functions of $\nu$. The function $\Omega_{i\nu}(B)$ computes radial Fourier transforms in $H_3$, satisfies $(\Box_{H_3} + \nu^2 + 1)\Omega_{i\nu} = 0$, and is given explicitly by

$$\Omega_{i\nu}(B) = \frac{1}{4\pi^2} \frac{\nu \sin \nu B}{\sinh B}.$$

Whenever the AdS phase satisfies $|\Delta| \ll 1$, the full cross section is well approximated by a single Reggeon exchange, and we may write

$$\sigma(s, \rho, \bar{\rho}, \mathbf{b}) \simeq 2\,\mathrm{Im}\Delta(S, B). \tag{10}$$

In this case, the integral over the impact parameter $\mathbf{b}$ can be explicitly performed. In fact, using the Regge representa-

[1] We take the AdS quantities $S$ and $B$ to be dimensionless, measured in units of the AdS radius.

[2] In this paper, in order to have a uniform notation, we use slightly different conventions than in [9,10]. In particular, $\Delta = -\pi\Gamma_{\text{there}}$ and $\beta_{\text{here}} = -\pi\beta_{\text{there}}$.

tion (9) for the phase shift, together with[3]

$$\int d^2\mathbf{b}\Omega_{i\nu}(B) = \frac{1}{2\pi}\rho\bar{\rho}\left(\frac{\bar{\rho}}{\rho}\right)^{-i\nu},$$

coming from the integral representation [10]

$$\Omega_{i\nu}(B) = \frac{\nu^2}{4\pi^3}\int d^2\mathbf{z}\left(\frac{\rho}{\rho^2+(\mathbf{b}-\mathbf{z})^2}\right)^{1+i\nu}\left(\frac{\bar{\rho}}{\bar{\rho}^2+\mathbf{z}^2}\right)^{1-i\nu},$$

we may evaluate the cross section $\sigma(s,\rho,\bar{\rho})$ to be

$$\sigma(s,\rho,\bar{\rho}) \simeq \frac{\rho\bar{\rho}}{2\pi N^2}\,\mathrm{Im}\int d\nu\beta(\nu)(s\rho\bar{\rho})^{j(\nu)-1}\left(\frac{\bar{\rho}}{\rho}\right)^{-i\nu}. \tag{11}$$

## II. THE CROSS SECTION DEEP INTO SATURATION

At fixed AdS energy squared $S$, the phase $\Delta(S,B)$ will, in general, vanish in the limit $B\to\infty$. On the other hand, as we approach smaller and smaller impact parameters, $\Delta$ will, in general, grow and reach saturation at $B\simeq \mathrm{B}_s(S)$, where $\Delta$ is of order one.

We will be mostly interested in weakly coupled gauge theories, where the phase is predominantly imaginary [12].[4] In this case, saturation is reached at[5]

$$2\,\mathrm{Im}\Delta(S,\mathrm{B}_s(S)) \simeq 1.$$

A typical plot of the saturation line in the $(B,\ln S)$ plane is given in Fig. 2. In particular, for large $S$ we have the linear relation

$$\mathrm{B}_s(S) \simeq \omega\ln S + \cdots, \tag{12}$$

where $\cdots$ represents subleading terms in $S$. This can be shown, as is customary [17], by approximating the integral in (9) at the saddle point $iB = j'(\nu)\ln S$. Saturation is then reached when the phase in (9) vanishes at the saddle—i.e. when $(1+i\nu_s)\mathrm{B}_s = (j(\nu_s)-1)\ln S$. These conditions imply that

$$\omega = -ij'(\nu_s),$$

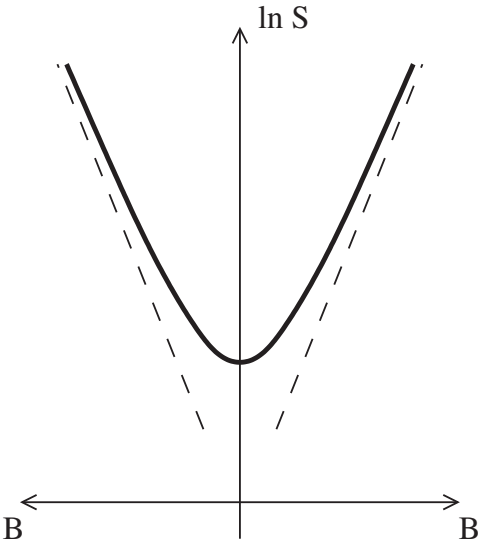


FIG. 2. Saturation line $\mathrm{B}_s(S)$ in the $B-\ln(S)$ plane. As we increase $S$, the saturation line starts at a minimal value of $S$ of the order of $\bar{\alpha}_s^{-1}$ and reaches the asymptotic linear behavior, shown with a dashed line, for large $S$. We extended the graph to the left of the $B=0$ axis symmetrically, drawing the mirror image of the saturation line. This is convenient, since $B=B(\rho,\bar{\rho},b)$ is invariant under $\rho\leftrightarrow\bar{\rho}$ and we wish to show separately regions with $\rho>\bar{\rho}$ and $\rho<\bar{\rho}$.

where the saturation saddle point $\nu_s$ is defined in terms of the Regge trajectory $j(\nu)$ by

$$(1+i\nu_s)\omega = j(\nu_s)-1.$$

The cross section $\sigma(s,\rho,\bar{\rho})$ near saturation $|\ln(\bar{\rho}/\rho)| \gtrsim \mathrm{B}_s(s\rho\bar{\rho})$ exhibits geometric scaling [18]. More precisely, the integral (11) has a leading behavior given by

$$\sigma(s,\rho,\bar{\rho}) \sim \bar{\rho}^2\tau^{-(1+i\nu_s)((1-\omega)/2)}, \tag{13}$$

where we have defined the scaling variable

$$\tau = \frac{\bar{\rho}^2}{\rho^2}(s\rho^2)^{-(2\omega/1-\omega)}. \tag{14}$$

On the other hand, we are interested in the analysis of the cross section $\sigma(s,\rho,\bar{\rho})$ deep inside saturation, that is, for

$$|\ln(\bar{\rho}/\rho)| \lesssim \mathrm{B}_s(s\rho\bar{\rho}). \tag{15}$$

In this case, the integral (8) is dominated by the region $B\lesssim \mathrm{B}_s$, where we may replace $\sigma(s,\rho,\bar{\rho},\mathbf{b})\simeq 1$. This situation corresponds to a simple black disk in AdS space, even though this is less transparent from the four-dimensional perspective. We then obtain the approximate expression for the cross section

$$\sigma(s,\rho,\bar{\rho}) \simeq 2\pi\rho\bar{\rho}\int_{|\ln(\bar{\rho}/\rho)|}^{\mathrm{B}_s} dB\sinh B$$
$$\simeq \pi\rho\bar{\rho}\left[2\cosh\mathrm{B}_s(s\rho\bar{\rho}) - \frac{\rho}{\bar{\rho}} - \frac{\bar{\rho}}{\rho}\right]. \tag{16}$$

[3]In order to correctly compute the normalization of this Fourier transform, as well as of the ones in the remainder of this paper, it is safest to compute at nonzero momentum transfer and then take the limit $\mathbf{q}\to\mathbf{0}$.

[4]On the other hand, at strong coupling and for large impact parameters, the phase shift is predominantly real and is given by the gravi-Reggeon exchange in AdS space. Studies of DIS in this regime include Ref. [13]. Saturation effects at strong coupling have also been analyzed in [14], and a conjectured relation to black hole formation was put forward in [15].

[5]Note that it is usually believed that, when $\mathrm{Im}\Delta\simeq 1$, nonlinear Balitsky-Kovchegov (BK) corrections to $\Delta$ of order $N^{-4}$ due to fan diagrams also become relevant [16]. As long as those corrections are negligible for impact parameters larger than the saturation line, they are irrelevant in the discussion which follows, since they will predominantly affect the phase shift in the black disk region.

Moreover, when $S = s\rho\bar{\rho}$ is large and we are in the linear regime (12), we have the simpler approximate expression

$$\sigma(s, \rho, \bar{\rho}) \simeq \pi\rho\bar{\rho}\left[(s\rho\bar{\rho})^{\omega} + (s\rho\bar{\rho})^{-\omega} - \frac{\rho}{\bar{\rho}} - \frac{\bar{\rho}}{\rho}\right], \quad (17)$$

where we neglect any subleading term in (12). Note that, for $\mathrm{B_s} \gg |\ln(\bar{\rho}/\rho)| \gg 1$, Eq. (17) is dominated by the first term, and we obtain

$$\sigma(s, \rho, \bar{\rho}) \sim \bar{\rho}^2 \tau^{-(1-\omega/2)},$$

to be contrasted with (13), valid near saturation. Finally note that, even in the deeply saturated region, the cross section $\sigma(s, \rho, \bar{\rho})$ grows with $s$ with a power law, violating the Froissart bound. Recall though that (17) has been derived by assuming an exact conformal symmetry and that, in a conformal theory, the Froissart bound is not relevant since there is no mass scale.

For the sake of clarity, let us discuss a specific example, which is at the same time simple and instructive, since it contains most of the relevant physics. We will work with the maximally superconformal version of QCD, $\mathcal{N} = 4$ super Yang-Mills with $SU(N)$ gauge group, and we will consider the scalar operators $\mathcal{O}_1 = \mathrm{Tr}(Z^2)$ and $\mathcal{O}_2 = \mathrm{Tr}(W^2)$ of dimension $\Delta_1 = \Delta_2 = 2$, with $Z$ and $W$ two of the three complex adjoint scalars of the theory. To leading order in $\bar{\alpha}_s$, we have the well known Balitsky, Fadin, Kuraev, and Lipatov (BFKL) result [12]

$$j(\nu) \simeq 1 + \bar{\alpha}_s\left(2\Psi(1) - \Psi\left(\frac{1 + i\nu}{2}\right) - \Psi\left(\frac{1 - i\nu}{2}\right)\right)$$

and [10]

$$\beta(\nu) \simeq i16\pi^4\bar{\alpha}_s^2 \frac{\tanh\frac{\pi\nu}{2}}{\nu(1 + \nu^2)^2}. \quad (18)$$

At vanishing $\ln S$, the integral (9) can be explicitly computed to be

$$\Delta(S = 1, B) = \frac{i}{3}\alpha_s^2\left[(6B^2 + 12B - \pi^2)\frac{e^{-B}}{\sinh B} - 12\ln(1 - e^{-2B}) + \frac{6}{\tanh B}\mathrm{Li}_2(e^{-2B})\right].$$

In particular, we see that at $B = 0$ we have $2\,\mathrm{Im}\Delta(S = 1, B = 0) \simeq 6.6\alpha_s^2$, which for a typical value of $\alpha_s$ is well below saturation. At $B = 0$ the saturation line starts for $\bar{\alpha}_s \ln S \simeq 1$, as can be seen from the integral expression (9) for the phase. The asymptotic linear regime (12) is reached for $\ln S \gtrsim 2/\bar{\alpha}_s$, with $i\nu_s \simeq 0.26$ and

$$\omega \simeq 2.44\bar{\alpha}_s.$$

The above are clearly leading order results. However, as we shall explain in more detail in the next section, the experimental value of $\omega$ in DIS experiments is lower. For example, in the analysis of [19], one finds $\omega \simeq 0.14$, since the scaling variable $\tau$ has the form (14) with $2\omega/(1 - \omega) \simeq 0.32$. Therefore, as is well known, next to leading order corrections to the leading BFKL results (which also distinguish between QCD and its supersymmetric extensions) are important to match to experiment.

## III. DEEP INELASTIC SCATTERING IN QCD AT SMALL $x$

We now explore the phenomenological consequences of our results on deeply saturated cross sections for DIS in QCD at small Bjorken $x$. Throughout the discussion, we shall assume that we are working in the conformal setting, thus neglecting the running of the coupling constant and all quark masses. We will associate the scalar operators $\mathcal{O}_1$ and $\mathcal{O}_2$, respectively, to the photon and the proton. Note that, deep into saturation, the spin of the external particles plays a minor role, since amplitudes are dominated by the black disk region with $\sigma(s, \rho, \bar{\rho}, \mathbf{b}) \simeq 1$. As usual, $Q^2$ is the photon virtuality and $s \simeq Q^2/x$. Moreover, the scale $\bar{Q}$ will now represent a phenomenological parameter, related to the proton wave function, of the order of the relevant proton scales. The wave functions $f_1, f_3$ and $f_2, f_4$ are localized, respectively, around $\rho \sim Q^{-1}$ and $\bar{\rho} \sim \bar{Q}^{-1}$. Therefore, the total cross section $\Sigma(s, Q, \bar{Q})$ in (6) can be approximately computed using the saturated cross section $\sigma(s, \rho, \bar{\rho})$ in (16) whenever

$$|\ln(Q/\bar{Q})| \lesssim \mathrm{B}_s(s/Q\bar{Q}). \quad (19)$$

Moreover, for large $s/Q\bar{Q}$, the saturation line $\mathrm{B}_s(S)$ is approximately linear, and $\sigma(s, \rho, \bar{\rho})$ is given by the simple expression (17). In this case, we may easily compute the radial integrals in (6) since, on purely dimensional grounds, we must have

$$\int \frac{d\rho}{\rho^3} f_1(\rho) f_3(\rho) \rho^{\zeta} = Q^{-\zeta}\gamma(\zeta)$$

for some constants $\gamma(\zeta)$ of order unity and similarly for the proton wave functions. Hence, in the deeply saturated regime at high $s/Q\bar{Q}$, we expect a rather simple form for the total cross section $\Sigma(s, Q, \bar{Q})$. Recalling that the cross section $\Sigma$ is proportional to $Q^{-2}F_2$, where $F_2(x, Q^2)$ is the usual DIS proton structure function, we obtain

$$F_2(x, Q^2) \simeq c\frac{Q}{\Lambda}\left[\left(\frac{Q}{x\Lambda}\right)^{\omega} + \left(\frac{Q}{x\Lambda}\right)^{-\omega}\right] - \tilde{c}\frac{Q}{\tilde{\Lambda}}\left[\frac{Q}{\tilde{\Lambda}} + \frac{\tilde{\Lambda}}{Q}\right], \quad (20)$$

where the constants $c$ and $\tilde{c}$ and the scales $\Lambda$ and $\tilde{\Lambda}$ are the only remnants of our lack of precise knowledge of the scattering radial wave functions. In particular, $\Lambda$ and $\tilde{\Lambda}$ will be of the same order as $\bar{Q}$. Had we included the spin of the particles in the discussion, the parameters $c$, $\tilde{c}$, $\Lambda$, and $\tilde{\Lambda}$ would carry also this kinematical information. The exponent $\omega$ is, on the other hand, universal and depends uniquely on the spin of the Pomeron. Note that, since $\omega \ll 1$, the constants of order unity coming from the first two

terms of (17) are essentially identical, and we may safely take

$$\Lambda \simeq \bar{Q}$$

in the first approximation.

As in (17), when $B_s(s/Q\bar{Q}) \gg |\ln(Q/\bar{Q})| \gg 1$, the cross section $\Sigma$ is dominated by the first term in (20) and exhibits the geometric scaling

$$\Sigma \sim \frac{1}{\bar{Q}^2}\tau^{-(1-\omega/2)}, \tag{21}$$

where we define the scaling variable $\tau$ as usual as [18]

$$\tau = \frac{Q^2}{Q_s^2}, \qquad Q_s^2 = \bar{Q}^2\left(\frac{1}{x}\right)^{(2\omega/1-\omega)}.$$

Recall that the power of $1/x$ in the saturation scale $Q_s^2$ is observed experimentally, following [19], to be given by $2\omega/(1-\omega) = 0.321 \pm 0.056$, so that

$$\omega = 0.138 \pm 0.021. \tag{22}$$

Deep into saturation, we predict that $\Sigma$ evolves with $\tau$ with the specific exponent in (21), which is *uniquely* fixed by the measurement of $\omega$ at the saturation scale $Q_s^2$. This has to be contrasted with the behavior of $\Sigma$ near saturation following from (13), where the exponent of $\tau$ is *not* fixed uniquely by $\omega$.

We wish to test this prediction against the available experimental data on $F_2(x, Q^2)$. Measurements have been performed at values of $x$ and $Q^2$ shown in Fig. 3, as discussed in [20], which collects all available data from [21]. In this figure, we present the data in the $\ln Q - \ln Q/x$ plane, with all energy scales measured in GeV from now on. These are the natural variables to discuss saturation, since they enter directly into (19). We will fit the available $F_2$ values using (20) in its plausible region of validity. First of all, we will take

$$Q > Q_{\min},$$

with $Q_{\min} \sim 1$ GeV so that, in the first approximation, the running of the coupling can be neglected. Second, we wish to choose points inside the saturation line (19). The exact determination of this line depends crucially on the phenomenological parameter $\bar{Q}$ and, in turn, on the strongly coupled dynamics of the proton. We expect the value of $\bar{Q}$ to be in the range of available scales—i.e. the QCD scale and the proton mass. Assuming that radial wave functions are localized around $\rho \sim Q^{-1}$ and $\bar{\rho} \sim \bar{Q}^{-1}$, the saturation line in the $\ln Q - \ln Q/x$ plane is then given by the saturation line for the AdS phase $\Delta$ shown in Fig. 2, where we replace $B$ and $\ln S$, respectively, by $|\ln Q/\bar{Q}|$ and $\ln Q/(x\bar{Q})$. In practice, this amounts to drawing the saturation line of Fig. 2 onto Fig. 3, offsetting the origin along the line $x = 1$ by $\ln\bar{Q}$. We shall then take points with

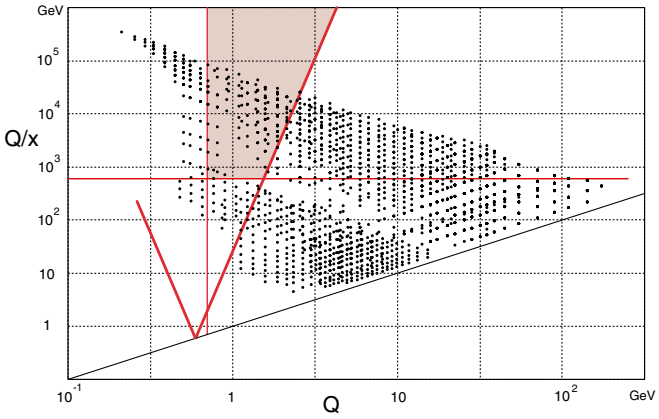


FIG. 3 (color online). Shown are the available measurements of $F_2(x, Q^2)$ in [21], in the $\log_{10}(Q) - \log_{10}(Q/x)$ plane, with energies measured in GeV. All points lie above the line $x = 1$. Shown also is the shaded region of points considered when analyzing (20). It corresponds to the region delimited by the vertical line, setting $Q > Q_{\min}$, the horizontal one, setting $\log_{10}(Q/x\bar{Q}) > \eta$, and the asymptotic linear saturation line. This is shown with a thicker line and is obtained by offsetting the graph in Fig. 2 by $\log_{10}(\bar{Q})$ along the $x = 1$ line.

$$\omega \ln\frac{Q}{x\bar{Q}} > \ln\frac{Q}{\bar{Q}} \qquad (\bar{Q} \sim 0.2\text{–}1 \text{ GeV}).$$

Third, we wish to consider data points with high values of $Q/(\bar{Q}x)$, so as to be into the linear regime of the saturation line. As explained in the previous section, the leading order BFKL analysis suggests that the linear regime starts around $\ln S \gtrsim 2/\bar{\alpha}_s$, so that we shall take data with

$$\frac{Q}{\bar{Q}x} \gtrsim 10^{\eta} \qquad (\eta \gtrsim 3).$$

To proceed, let us choose $Q_{\min} = 0.7$ GeV, $\bar{Q} = 0.6$ GeV, and $\eta = 3$. We will show later that the main results are insensitive to this specific choice. The selected data are shown in the shaded region of Fig. 3. We shall test our theoretical prediction against the real data in [21] as well as against the very accurate neural network interpolation to world DIS data in [22]. In particular, we shall minimize the average square deviation of the data from the predicted theoretical form (20). Since the parameters $c$, $\tilde{c}$, and $\tilde{c}/\tilde{\Lambda}^2$ enter linearly in (20), minimization reduces to a linear system parametrized by the single parameter $\omega$.

As a function of $\omega$, the parameters $c$, $\tilde{c}$, and $\tilde{c}/\tilde{\Lambda}^2$ are easily determined both for real as well as for simulated data. As is clear from (20), the parameter $\omega$ controls the growth of $F_2$ as $1/x$ increases. More precisely, at fixed $Q$, the coefficients $c$ and $\omega$ determine the slope as well as the convexity of the function $F_2$ in the experimental region of interest, shaded in Fig. 3. Unfortunately, the relevant kine-

matics is on the boundary of the currently accessible experimental settings, resulting in data of relatively poor quality with large experimental uncertainty. This is reflected in the fact that the error function, although it presents a minimum for $\omega \simeq 0.136$, is essentially constant in the range 0.1–0.17 plotted in Fig. 4. On the other hand, as shown in the same figure, if we use the more accurate simulated function $F_2$ computed at the same values of $x$ and $Q^2$ available in the real data [22], we obtain a rather sharp minimum for the error function at

$$\omega \simeq 0.126.$$

Therefore, from now on, we shall determine the optimal value of $\omega$ using the simulated data only. At this point we wish to emphasize that this value of $\omega$, obtained from data inside the saturated kinematical region, is within the experimental range $\omega = 0.138 \pm 0.021$, obtained independently from geometric scaling. The values for the other relevant parameters can be determined to be $\tilde{\Lambda} \simeq 1.0$ GeV, $c \simeq 0.13$, and $\tilde{c} \simeq 0.14$ for the real data and $\tilde{\Lambda} \simeq 1.0$ GeV, $c \simeq 0.11$, and $\tilde{c} \simeq 0.08$ for the simulated one.

The real data are presented in Figs. 5 and 6, where we show the data together with the theoretical curves from (20). We plot $F_2/Q$ as a function of $\log_{10}Q$, and each graph contains data points with values of $\log_{10}(Q/x)$ in the range $Y \pm 0.1$, for $2 \leq Y \leq 5$ in increments of 0.2. Theoretical curves are shown in red for both the minimal and the maximal values of $\log_{10}(Q/x)$. Finally, the shaded area corresponds to the region delimited by the choice of parameters $\bar{Q}$, $\eta$, and $Q_{\min}$, as also shown in Fig. 3. Analogously, Figs. 7 and 8 show the simulated data.

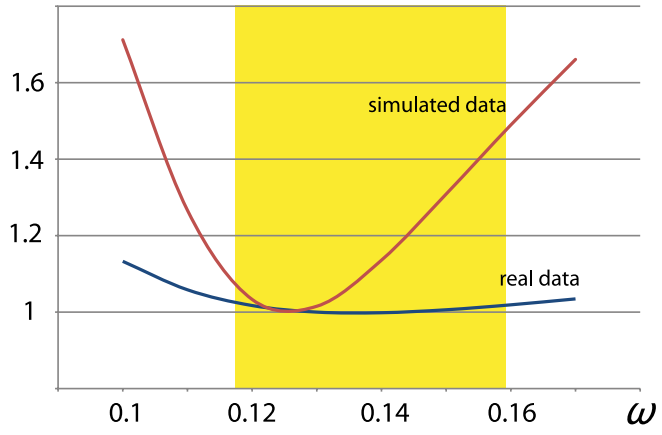


FIG. 4 (color online). Error functions for real and simulated data, plotted as a function of $\omega$. For comparison, both functions have been normalized to 1 at their respective minima. The error for the simulated data exhibits a sharp minimum, while the corresponding error for real data is more insensitive to $\omega$, due to a large experimental uncertainty. We therefore choose to fix $\omega$ using the simulated data. The yellow stripe corresponds to the range $\omega = 0.138 \pm 0.021$ obtained from geometric scaling.

Let us note that the AdS black disk form of the structure function given in (20), with the above choice of parameters, approximates the available real data with an average 6% accuracy in the rather large region of parameter space $0.5 < Q^2 < 10$ and $x < 10^{-2}$.

Because of uncertainty on the precise location of the saturation line, we have repeated the analysis with different values of $\bar{Q}$, $Q_{\min}$, and $\eta$, to test the robustness of the predicted value for $\omega$. Within the range $0.7 < Q_{\min} < 1$ and $0.3 < \bar{Q} < 1$, the fitted value for $\omega$ varies from 0.090 to 0.152, as shown in Table I, thus mostly within the predicted range (the optimal value of $\omega$ is rather insensitive to the choice of $\eta > 3$ which we keep fixed). Note that, although the first two entries of Table I are outside the predicted range, they are based on a very small number of data points.

As already stressed, available data are on the boundary of the deeply saturated region, and one would need to reach higher energies in order to better test these predictions. Possibly, future data from LHC will be of use to confirm the above results.

## IV. RELATION TO THE DIPOLE FORMALISM

We will conclude this paper by discussing the relation between the above results and the dipole formalism [23], which is usually employed in the analysis of saturation effects. In this context, it is customary to analyze the so-called dipole-dipole cross section $\sigma_{\rm DD}(s, \mathbf{r}, \bar{\mathbf{r}}, \mathbf{b})$ instead of $\sigma(s, \rho, \bar{\rho}, \mathbf{b})$, with the full cross section $\Sigma(s, Q, \bar{Q})$ given by integrals over the dipole transverse orientations $\mathbf{r}$ and $\bar{\mathbf{r}}$

$$\frac{2}{(2\pi)^2}\int \frac{d^2\mathbf{r}}{\mathbf{r}^4}\frac{d^2\bar{\mathbf{r}}}{\bar{\mathbf{r}}^4} W(\mathbf{r})\sigma_{\rm DD}(s, \mathbf{r}, \bar{\mathbf{r}})\bar{W}(\bar{\mathbf{r}}),$$
$$\sigma_{\rm DD}(s, \mathbf{r}, \bar{\mathbf{r}}) = \int d^2\mathbf{b}\,\sigma_{\rm DD}(s, \mathbf{r}, \bar{\mathbf{r}}, \mathbf{b}), \tag{23}$$

where $W(\mathbf{r})$ and $\bar{W}(\bar{\mathbf{r}})$ are the so-called dipole impact factors.

Let us first note that, although the dipole formalism is quite useful due to its intuitive physical description of the high energy process and of the linear BFKL and nonlinear BK evolutions [16], it is not well suited for the discussion of unitarization, since the natural object which satisfies the unitarity constraint $0 \leq \sigma \leq 2$ is $\sigma(s, \rho, \bar{\rho}, \mathbf{b})$, instead of $\sigma_{\rm DD}(s, \mathbf{r}, \bar{\mathbf{r}}, \mathbf{b})$. This fact is quite clear in gauge theories which are exactly conformal, like $\mathcal{N} = 4$ super Yang-Mills, where the dipole formalism can still be applied (as well as the BK equation, which is explicitly conformally invariant). In this case, the theory has no asymptotic states or an $S$ matrix to which to apply the usual unitarity constraints. Moreover, even in a confining theory like QCD, which possesses asymptotic states, the dipole state is not a single particle state at infinity and therefore does not enter in a usual $S$-matrix element. In fact, in the standard discussions of DIS at small $x$, the dipole picture is often used

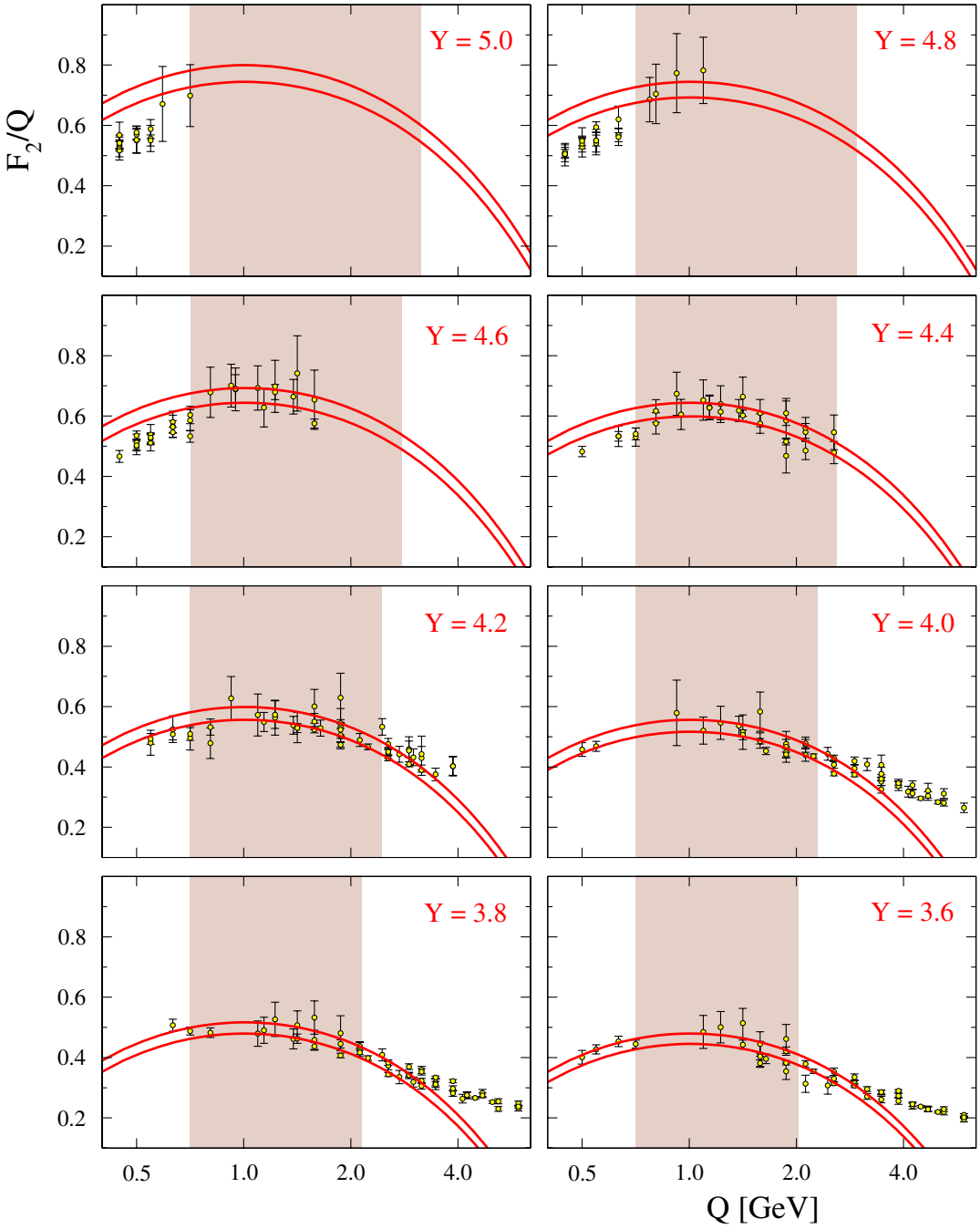


FIG. 5 (color online). Real data $F_2/Q$ as a function of $Q$. Each graph contains data points with values of $\log_{10}(Q/x)$ in the range $Y \pm 0.1$, for $3.6 \leq Y \leq 5$ in increments of 0.2. Theoretical curves are shown in red for both the minimal and the maximal values of $\log_{10}(Q/x)$. The shaded area corresponds to the region delimited by the choice of parameters $Q_{\min} = 0.7$ GeV, $\bar{Q} = 0.6$ GeV, and $\eta = 3$, as also shown in Fig. 3.

to describe the wave function of an off-shell spacelike photon.

At any rate, in order to make contact with the standard literature, we will briefly analyze, in what follows, the above expressions in the unsaturated regime of small AdS phase shift $|\Delta| \ll 1$.

Let us first analyze the impact factors $W(\mathbf{r})$ and $\bar{W}(\bar{\mathbf{r}})$, leaving to the second part of this section the discussion on $\sigma_{\mathrm{DD}}(s, \mathbf{r}, \bar{\mathbf{r}}, \mathbf{b})$ and on saturation in the context of the dipole formalism. We recall the BFKL representation of $\Delta$ analyzed in [10]. More precisely, to leading order in the coupling we have

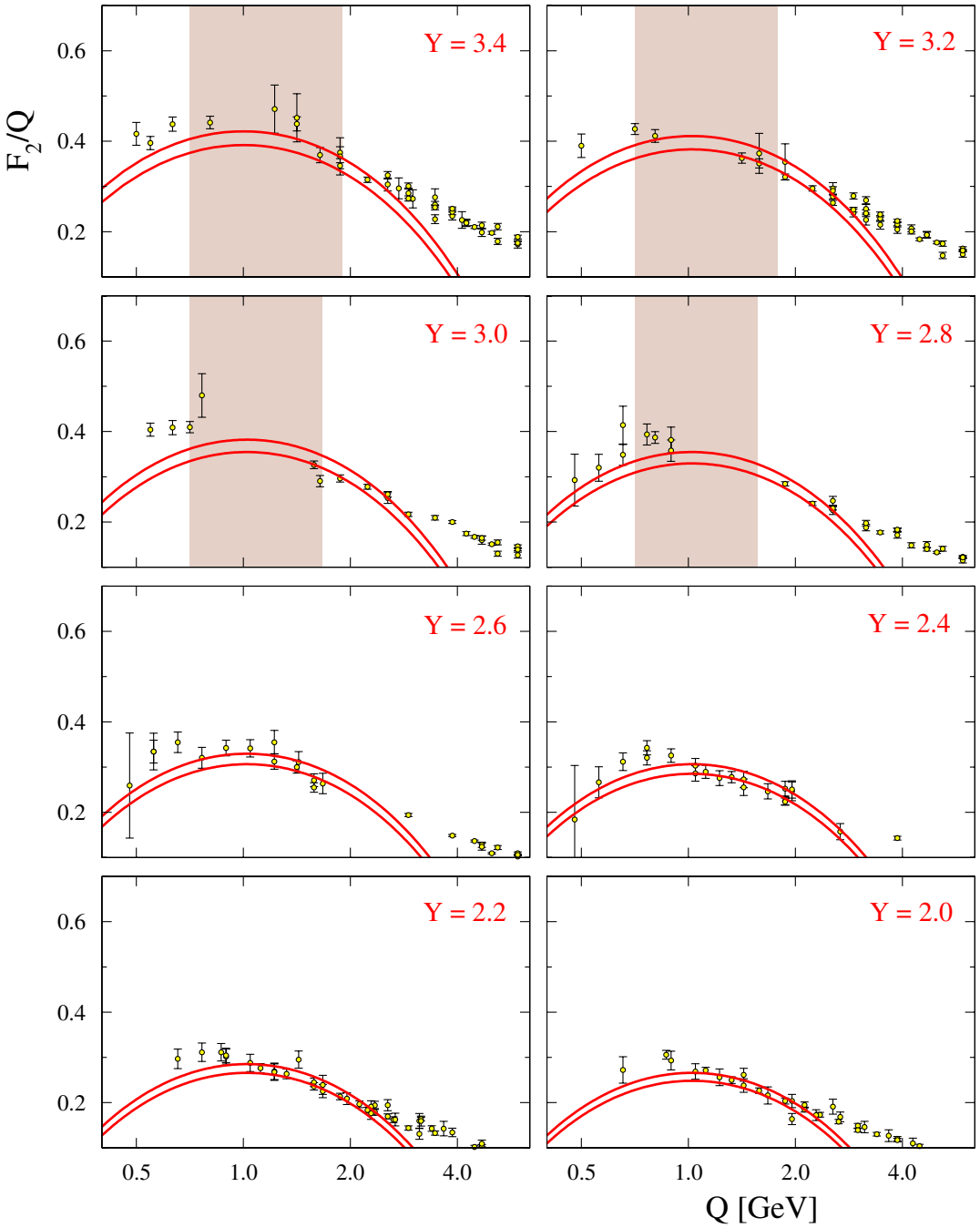


FIG. 6 (color online). Real data $F_2/Q$ as a function of $Q$. Each graph contains data points with values of $\log_{10}(Q/x)$ in the range $Y \pm 0.1$, for $2 \leq Y \leq 3.4$ in increments of 0.2. Theoretical curves are shown in red for both the minimal and the maximal values of $\log_{10}(Q/x)$. The shaded area corresponds to the region delimited by the choice of parameters $Q_{\min} = 0.7$ GeV, $\bar{Q} = 0.6$ GeV, and $\eta = 3$, as also shown in Fig. 3.

$$2\Delta = \frac{i}{N^2}\int \frac{d^2\mathbf{r}}{\mathbf{r}^4}\frac{d^2\bar{\mathbf{r}}}{\bar{\mathbf{r}}^4} d^2\mathbf{y} d^2\bar{\mathbf{y}} W(\rho, \mathbf{r}, \mathbf{x}-\mathbf{y}) F(\mathbf{r}, \bar{\mathbf{r}}, \mathbf{y}-\bar{\mathbf{y}}) \times \bar{W}(\bar{\rho}, \bar{\mathbf{r}}, \bar{\mathbf{x}}-\bar{\mathbf{y}}),$$

with $\mathbf{b} = \mathbf{x} - \bar{\mathbf{x}}$. The impact factor $W$ depends on the point $\rho$, $\mathbf{x}$ in $H_3$ and on the two intermediate points $\mathbf{y} \pm \mathbf{r}/2$ on the boundary of $H_3$, as represented in Fig. 9. Similar comments apply to the impact factor $\bar{W}$. Moreover, $F(\mathbf{r}, \bar{\mathbf{r}}, \mathbf{y} - \bar{\mathbf{y}})$ is the leading order two-gluon exchange kernel from $\mathbf{y} \pm \mathbf{r}/2$ to $\bar{\mathbf{y}} \pm \bar{\mathbf{r}}/2$. Integrating against

$$2\int d^2\mathbf{b} \int \frac{d\rho}{\rho^3} f_1(\rho) f_3(\rho) \int \frac{d\bar{\rho}}{\bar{\rho}^3} f_2(\bar{\rho}) f_4(\bar{\rho})$$

and using the approximate relation (10) valid in the small

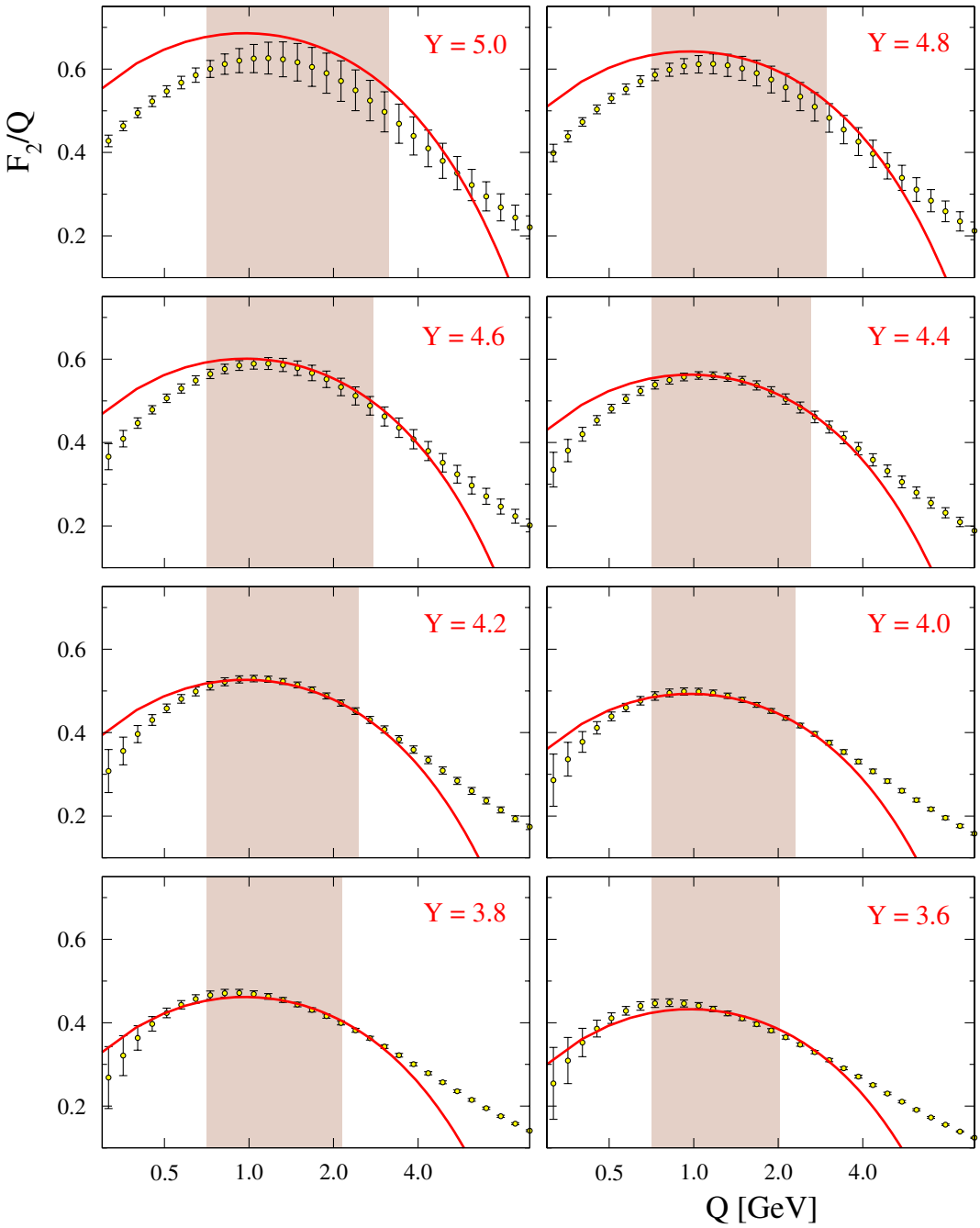


FIG. 7 (color online). The same as Fig. 5 for the simulated function $F_2$ computed at evenly spaced values of $Q$ for fixed $Y = \log_{10}(Q/x)$.

phase regime, we obtain an expression of the form (23), where

$$\sigma_{\mathrm{DD}}(s, \mathbf{r}, \bar{\mathbf{r}}) \simeq c\bar{c}\frac{(2\pi)^2}{N^2}\,\mathrm{Re}\int d^2\mathbf{w} F(\mathbf{r}, \bar{\mathbf{r}}, \mathbf{w}), \qquad W(\mathbf{r}) = \frac{1}{c}\int\frac{d\rho}{\rho^3} f_1(\rho) f_3(\rho)\int d^2\mathbf{w} W(\rho, \mathbf{r}, \mathbf{w}), \tag{24}$$

and similarly for $\bar{W}(\bar{\mathbf{r}})$. The constants $c$ and $\bar{c}$ are fixed by the normalization conditions

$$\frac{1}{2\pi}\int\frac{d^2\mathbf{r}}{\mathbf{r}^4} W(\mathbf{r}) = \frac{1}{2\pi}\int\frac{d^2\bar{\mathbf{r}}}{\bar{\mathbf{r}}^4}\bar{W}(\bar{\mathbf{r}}) = 1$$

analogous to (5).

Let us discuss the impact factor $W$ in detail. As shown in [10], conformal invariance highly constrains $W(\rho, \mathbf{r}, \mathbf{w})$ to be a function of the unique cross ratio

$$\frac{\mathbf{r}^2\rho^2}{[\rho^2 + (\mathbf{w} - \frac{\mathbf{r}}{2})^2][\rho^2 + (\mathbf{w} + \frac{\mathbf{r}}{2})^2]},$$

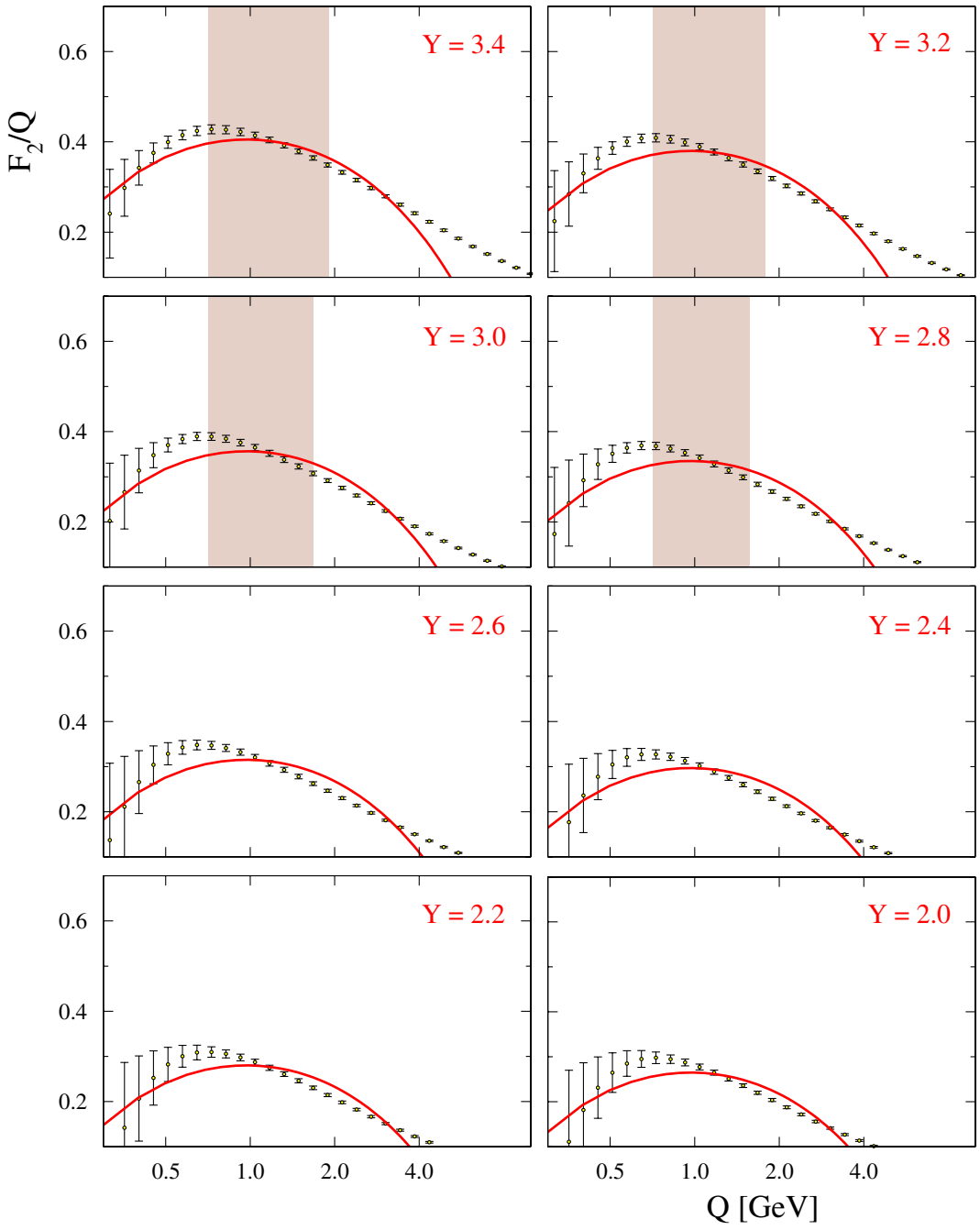


FIG. 8 (color online). The same as Fig. 6 for the simulated function $F_2$ computed at evenly spaced values of $Q$ for fixed $Y = \log_{10}(Q/x)$.

which can be conveniently written in the following integral representation[6]:

$$\frac{1}{64\pi^5}\int d\nu\nu^2(1+\nu^2)\frac{\Gamma^2(\frac{1-i\nu}{2})}{\Gamma(1-i\nu)}W(\nu) \times \int d^2\mathbf{z}\left(\frac{\rho}{\rho^2+(\mathbf{w}-\mathbf{z})^2}\right)^{1+i\nu} \times \left(\frac{\mathbf{r}^2}{(\mathbf{z}-\frac{\mathbf{r}}{2})^2(\mathbf{z}+\frac{\mathbf{r}}{2})^2}\right)^{(1-i\nu/2)}, \quad (25)$$

where the transforms $W(\nu)$ and $\bar{W}(\nu)$ determine the Regge

[6]In the notation of [10], $W(\nu)$ is given by $V(\nu)/V_{\min}(\nu,1)$, with $V(\nu)$ the impact factor for the full amplitude and with $V_{\min}(\nu,1) = \Gamma(\frac{2\Delta_1-1+i\nu}{2})\Gamma(\frac{2\Delta_1-1-i\nu}{2})/(\Gamma(\Delta_1)\Gamma(\Delta_1-1))$, where $\Delta_1$ is the dimension of the external operator $\mathcal{O}_1$, and similarly for $\bar{W}$.

TABLE I. Number of experimentally available data points $n$ and predicted value of $\omega$ for different values of $\bar{Q}$ and $Q_{\min}$.

| $\bar{Q}$ | $Q_{\min}$ | $\eta$ | $n$ | $\omega$ |
|---|---|---|---|---|
| 0.3 | 0.7 | 3 | 58 | 0.104 |
| 0.3 | 1 | 3 | 23 | 0.090 |
| 0.6 | 0.7 | 3 | 138 | 0.126 |
| 0.6 | 1 | 3 | 104 | 0.130 |
| 1 | 0.7 | 3 | 200 | 0.141 |
| 1 | 1 | 3 | 171 | 0.152 |

residue $\beta(\nu)$ to be

$$\beta(\nu) = \frac{i}{4\nu} W(\nu) \tanh(\pi\nu/2) \bar{W}(\nu).$$

Moving to momentum space in the transverse $\mathbb{E}^2$ plane by integrating against $\int d^2\mathbf{w}$, we obtain

$$\frac{1}{32\pi^3} \int d\nu (1+\nu^2) W(\nu) \times \int_0^1 \frac{d\zeta}{\sqrt{\zeta(1-\zeta)}} \rho|\mathbf{r}| \left(\frac{\zeta(1-\zeta)\mathbf{r}^2}{\rho^2}\right)^{(i\nu/2)}, \quad (26)$$

where $\zeta$ is the Feynman parameter related to the denominators in the last parentheses of (25).

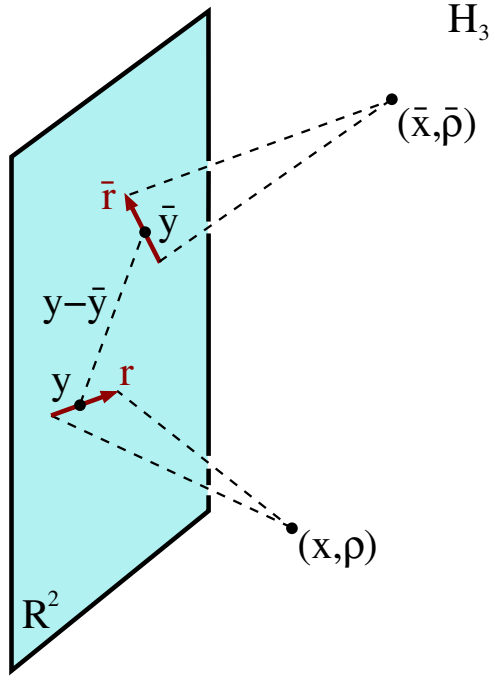


FIG. 9 (color online). Relation to dipole formalism. While the dipole-dipole cross section $\sigma_{\mathrm{DD}}(s, \mathbf{r}, \bar{\mathbf{r}}, \mathbf{y}-\bar{\mathbf{y}})$ depends on four points in $\mathrm{R}^2$, the cross section $\sigma(s, \rho, \bar{\rho}, \mathbf{x}-\bar{\mathbf{x}})$, which is the one constrained by unitarity, depends only on two points in $\mathrm{H}_3$. The role of the dipole vectors $\mathbf{r}$ and $\bar{\mathbf{r}}$ is now played by the radial coordinates $\rho$ and $\bar{\rho}$.

For concreteness, let us return to the specific example already discussed in Sec. II, with $\beta(\nu)$ given by (18). We have that $W(\nu) = 8\pi^2\bar{\alpha}_s/(1+\nu^2)$. Then $W(\mathbf{r})$ can be computed from (26), since the $\nu$ integral fixes $\rho = |\mathbf{r}|\sqrt{\zeta(1-\zeta)}$. After integrating against $c^{-1}\int d\rho\rho^{-3} f_1 f_3$, we obtain

$$W(\mathbf{r}) = \int_0^1 \frac{d\zeta}{\zeta(1-\zeta)} f_1(\sqrt{\zeta(1-\zeta)}|\mathbf{r}|) f_3(\sqrt{\zeta(1-\zeta)}|\mathbf{r}|),$$

with $c = \bar{\alpha}_s/2$. Using the fact that $f_i(\rho) = \sqrt{2} Q_i \rho^2 K_0(Q_i\rho)$ for $i = 1, 3$, we have just obtained the usual expression in terms of dipole wave functions [23].

To conclude this section, let us recall the form of the dipole-dipole cross section $\sigma_{\mathrm{DD}}(s, \mathbf{r}, \bar{\mathbf{r}})$, in the unsaturated case (24). It is given by the usual BFKL kernel

$$\sigma_{\mathrm{DD}}(s, \mathbf{r}, \bar{\mathbf{r}}) \simeq \frac{|\mathbf{r}||\bar{\mathbf{r}}|}{2\pi N^2} \int d\nu \frac{16\pi^3\bar{\alpha}_s^2}{(1+\nu^2)^2} (s|\mathbf{r}||\bar{\mathbf{r}}|)^{j(\nu)-1} \left|\frac{\bar{\mathbf{r}}}{\mathbf{r}}\right|^{-i\nu},$$

which should be compared with (11), with $\beta(\nu)$ given by (18). Recall also that the above expression is the zero momentum contribution to the full BFKL expression for $\sigma_{\mathrm{DD}}(s, \mathbf{r}, \bar{\mathbf{r}}, \mathbf{b})$ given by [24]

$$\sigma_{\mathrm{DD}}(s, \mathbf{r}, \bar{\mathbf{r}}, \mathbf{b}) \simeq \frac{i}{2\pi^2 N^2} \int d\nu \nu \alpha(\nu) \times (s|\mathbf{r}||\bar{\mathbf{r}}|)^{j(\nu)-1} \mathcal{T}_{i\nu}(\mathbf{r}, \bar{\mathbf{r}}, \mathbf{b}), \quad (27)$$

where

$$\alpha(\nu) = \frac{16\pi^3\bar{\alpha}_s^2}{(1+\nu^2)^2} \frac{\Gamma(1-i\nu)}{\Gamma(\frac{1-i\nu}{2})^2} \frac{\Gamma(\frac{1+i\nu}{2})^2}{\Gamma(1+i\nu)}$$

and where $\mathcal{T}_{i\nu}(\mathbf{r}, \bar{\mathbf{r}}, \mathbf{b})$ is the two-dimensional conformal partial wave of spin 0 and conformal dimension $1+i\nu$ at the four points $(\mathbf{b} \pm \mathbf{r})/2$, $(-\mathbf{b} \pm \bar{\mathbf{r}})/2$. Because of transverse conformal invariance, $\mathcal{T}_{i\nu}$ depends uniquely on the cross-ratio combinations

$$z\bar{z} = \frac{\mathbf{r}^2\bar{\mathbf{r}}^2}{(\mathbf{b} - \frac{\mathbf{r}}{2} + \frac{\bar{\mathbf{r}}}{2})^2 (\mathbf{b} + \frac{\mathbf{r}}{2} - \frac{\bar{\mathbf{r}}}{2})^2},$$

$$\frac{z\bar{z}}{(1-z)(1-\bar{z})} = \frac{\mathbf{r}^2\bar{\mathbf{r}}^2}{(\mathbf{b} - \frac{\mathbf{r}}{2} - \frac{\bar{\mathbf{r}}}{2})^2 (\mathbf{b} + \frac{\mathbf{r}}{2} + \frac{\bar{\mathbf{r}}}{2})^2}$$

and is given explicitly by

$$\mathcal{T}_{i\nu}(\mathbf{r}, \bar{\mathbf{r}}, \mathbf{b}) = (-z)^h (-\bar{z})^h F(h, h, 2h, z) F(h, h, 2h, \bar{z}),$$

$$h = \frac{1+i\nu}{2},$$

where $F$ is the hypergeometric function ${}_2F_1$.

The expression (27) should be confronted with $\sigma(s, \rho, \bar{\rho}, \mathbf{b})$ derived from Eqs. (9) and (10) in the limit of small AdS phase shift $|\Delta| \ll 1$:

$$\sigma(s,\rho,\bar{\rho},\mathbf{b}) \simeq \frac{i}{2\pi^2 N^2}\int d\nu\,\nu\,\mathrm{Im}\beta(\nu)S^{j(\nu)-1}\frac{e^{-i\nu B}}{\sinh B}. \tag{28}$$

Given the similarity of the expressions for $\sigma_{\mathrm{DD}}$ and $\sigma$, we may try to follow the program of Sec. II and consider the saturation region in the transverse impact parameter $\mathbf{b}$ space where, at fixed energy $s$ and dipole orientations $\mathbf{r}$ and $\bar{\mathbf{r}}$, the cross section $\sigma_{\mathrm{DD}}(s,\mathbf{r},\bar{\mathbf{r}},\mathbf{b})$ becomes greater than unity. On the other hand, this program cannot be carried out, in general. In fact, while the cross section $\sigma(s,\rho,\bar{\rho},\mathbf{b})$ depends, aside from energy, on a single conformal cross ratio $B$, the cross section $\sigma_{\mathrm{DD}}(s,\mathbf{r},\bar{\mathbf{r}},\mathbf{b})$ depends on energy and on two cross ratios $z$ and $\bar{z}$ which reflect the orientations of the two dipoles (the scalar quantities $\rho$ and $\bar{\rho}$ are replaced by the dipole transverse vectors $\mathbf{r}$ and $\bar{\mathbf{r}}$, respectively). Moreover, both $B$ and $\ln S$ enter exponentially in (28) and allow for a simple saddle approximation of the integral and for the determination of the saturation line as in (12). On the other hand, the dependence of the integrand in (27) on $z$ and $\bar{z}$ is now highly nontrivial, since it involves not only the norms but also the orientations of $\mathbf{r}$, $\bar{\mathbf{r}}$, and $\mathbf{b}$. Most importantly, it does not allow for a simple approximation of the integral at a saddle point and a simple determination of the saturation line.

The analysis of the saturation region for $\sigma_{\mathrm{DD}}$ can be carried out only in the limit $|\mathbf{r}|, |\bar{\mathbf{r}}| \ll |\mathbf{b}|$. In fact, in this limit, one may use the operator product expansion and obtain

$$\mathcal{T}_{i\nu}(\mathbf{r},\bar{\mathbf{r}},\mathbf{b}) \simeq \left(\frac{|\mathbf{r}||\bar{\mathbf{r}}|}{\mathbf{b}^2}\right)^{1+i\nu} \tag{29}$$

of the simple exponential form. Similarly, in the same limit $\rho, \bar{\rho} \ll |\mathbf{b}|$, one has $B \simeq \ln(\mathbf{b}^2/\rho\bar{\rho})$, and one may substitute in (28)

$$\frac{e^{-i\nu B}}{\sinh B} \simeq \left(\frac{\rho\bar{\rho}}{\mathbf{b}^2}\right)^{1+i\nu},$$

obtaining an expression analogous to (29). From here on we may follow the usual steps reviewed in Sec. II to determine the saturation radius, which is given, in general, by $\ln(\mathbf{b}^2/|\mathbf{r}||\bar{\mathbf{r}}|) \simeq \omega \ln(s|\mathbf{r}||\bar{\mathbf{r}}|)$, leading to a black disk cross section given by $\pi\mathbf{b}^2 \simeq \pi|\mathbf{r}||\bar{\mathbf{r}}|(s|\mathbf{r}||\bar{\mathbf{r}}|)^{\omega}$.

With this procedure we recover an expression analogous to the first term of (17) just as easily in the dipole formalism. On the other hand, as we already pointed out, the usual saddling argument works in (28) for generic values of $\rho$, $\bar{\rho}$, and $\mathbf{b}$. This fact allows us to determine the other terms in Eq. (17), which could not have been deduced in the dipole language. Note that the extra three terms in (17), and correspondingly in (20), are crucial in order to have a qualitatively good fit for the relevant $F_2$ data at hand. In fact, the expression for $F_2/Q$ exhibits a nontrivial dependence on $Q$ at fixed $Q/x$, which is qualitatively correctly captured by the third and fourth terms in (20) proportional to

$$-\frac{Q}{\tilde{\Lambda}} - \frac{\tilde{\Lambda}}{Q}.$$

These terms give a concave behavior with a maximum at $Q \simeq \tilde{\Lambda}$, which is a clear feature of the $F_2$ data, as can be seen from the plots in Figs. 5–8. A pure term of the form $(Q/x)^{\omega}$, as could be determined by the above arguments also in the usual dipole formalism, is clearly insufficient to reproduce the $Q$ dependence at fixed $Q/x$ inside the saturation region.

## ACKNOWLEDGMENTS

We thank João Viana Lopes and Giulia Galbiati for support with the data analysis, Andrea Banfi for discussions, and Markus Diehl for carefully reading the manuscript. L. C. is funded by the *Museo Storico della Fisica e Centro Studi e Ricerche "Enrico Fermi"* and is partially funded by INFN, by the MIUR-PRIN Contract No. 2005-024045-002, and by the EU Contract No. MRTN-CT-2004-005104. M. C. is partially funded by the FCT-CERN Grant No. POCI/FP/63904/2005. *Centro de Física do Porto* is partially funded by FCT through the POCI program.

[1] J. M. Maldacena, Adv. Theor. Math. Phys. **2**, 231 (1998).
[2] J. Polchinski and M. J. Strassler, Phys. Rev. Lett. **88**, 031601 (2002).
[3] R. C. Brower, J. Polchinski, M. J. Strassler, and C. I. Tan, J. High Energy Phys. 12 (2007) 005.
[4] L. Cornalba, M. S. Costa, J. Penedones, and R. Schiappa, J. High Energy Phys. 08 (2007) 019.
[5] L. Cornalba, M. S. Costa, J. Penedones, and R. Schiappa, Nucl. Phys. **B767**, 327 (2007).
[6] L. Cornalba, M. S. Costa, and J. Penedones, J. High Energy Phys. 09 (2007) 037.
[7] R. C. Brower, M. J. Strassler, and C. I. Tan, arXiv:0707.2408.
[8] R. C. Brower, M. J. Strassler, and C. I. Tan, arXiv:0710.4378.
[9] L. Cornalba, arXiv:0710.5480.
[10] L. Cornalba, M. S. Costa, and J. Penedones, J. High Energy Phys. 06 (2008) 048.
[11] S. S. Gubser, I. R. Klebanov, and A. M. Polyakov, Phys. Lett. B **428**, 105 (1998); E. Witten, Adv. Theor. Math. Phys. **2**, 253 (1998).
[12] V. S. Fadin, E. A. Kuraev, and L. N. Lipatov, Phys. Lett.

**60B**, 50 (1975); E. A. Kuraev, L. N. Lipatov, and V. S. Fadin, Sov. Phys. JETP **45**, 199 (1977); Ya. Ya. Balitsky and L. N. Lipatov, Sov. J. Nucl. Phys. **28**, 822 (1978).

[13] J. Polchinski and M. J. Strassler, J. High Energy Phys. 05 (2003) 012; C. A. Ballon Bayona, H. Boschi-Filho, and N. R. F. Braga, J. High Energy Phys. 03 (2008) 064; arXiv:0712.3530.

[14] Y. Hatta, E. Iancu, and A. H. Mueller, J. High Energy Phys. 01 (2008) 026.

[15] L. Alvarez-Gaume, C. Gomez, and M. A. Vazquez-Mozo, Phys. Lett. B **649**, 478 (2007); L. Alvarez-Gaume, C. Gomez, A. S. Vera, A. Tavanfar, and M. A. Vazquez-Mozo, Nucl. Phys. **B806**, 327 (2008).

[16] A. H. Mueller, arXiv:hep-ph/0111244.

[17] L. V. Gribov, E. M. Levin, and M. G. Ryskin, Phys. Rep. **100**, 1 (1983); E. Iancu and L. D. McLerran, Phys. Lett. B **510**, 145 (2001); A. H. Mueller, Nucl. Phys. **B558**, 285 (1999); A. H. Mueller and D. N. Triantafyllopoulos , Nucl. Phys. **B640**, 331 (2002); S. Munier and R. Peschanski, Phys. Rev. Lett. **91**, 232001 (2003); Phys. Rev. D **69**, 034008 (2004); **70**, 077503 (2004).

[18] A. M. Stasto, K. Golec-Biernat, and J. Kwiecinski, Phys. Rev. Lett. **86**, 596 (2001).

[19] F. Gelis, R. B. Peschanski, G. Soyez, and L. Schoeffel, Phys. Lett. B **647**, 376 (2007).

[20] L. Del Debbio, S. Forte, J. I. Latorre, A. Piccione, and J. Rojo (NNPDF Collaboration), J. High Energy Phys. 03 (2005) 080.

[21] M. Arneodo *et al.* (New Muon Collaboration), Nucl. Phys. **B483**, 3 (1997); A. C. Benvenuti *et al.* (BCDMS Collaboration), Phys. Lett. B **223**, 485 (1989); M. R. Adams *et al.* (E665 Collaboration), Phys. Rev. D **54**, 3006 (1996); M. Derrick *et al.* (ZEUS Collaboration), Z. Phys. C **72**, 399 (1996); J. Breitweg *et al.* (ZEUS Collaboration), Phys. Lett. B **407**, 432 (1997); Eur. Phys. J. C **7**, 609 (1999); S. Chekanov *et al.* (ZEUS Collaboration), Eur. Phys. J. C **21**, 443 (2001); J. Breitweg *et al.* (ZEUS Collaboration), Phys. Lett. B **487**, 53 (2000); C. Adloff *et al.* (H1 Collaboration), Nucl. Phys. **B497**, 3 (1997); Eur. Phys. J. C **13**, 609 (2000); **21**, 33 (2001); **19**, 269 (2001); **30**, 1 (2003).

[22] S. Forte, L. Garrido, J. I. Latorre, and A. Piccione, J. High Energy Phys. 05 (2002) 062; http://sophia.ecm.ub.es/nnpdf/.

[23] A. H. Mueller, Nucl. Phys. **B415**, 373 (1994); A. H. Mueller and B. Patel, Nucl. Phys. **B425**, 471 (1994); A. H. Mueller, Nucl. Phys. **B437**, 107 (1995).

[24] L. N. Lipatov, Phys. Rep. **286**, 131 (1997).